THE JOURNAL OF BIOLOGICAL CHEMISTRY VOL. 291, NO. 36, pp. 19184–19195, September 2, 2016

Aquaporin 4 as a NH_3 Channel*

Received for publication, May 25, 2016, and in revised form, July 8, 2016 Published, JBC Papers in Press, July 19, 2016, DOI 10.1074/jbc.M116.740217

Mette Assentoft[‡1,2], Shreyas Kaptan[§1,3], Hans-Peter Schneider[¶], Joachim W. Deitmer[¶4], Bert L. de Groot[§3], and Nanna MacAulay[‡5]

From the [‡]Department of Neuroscience and Pharmacology, University of Copenhagen, 2200 Copenhagen, Denmark, [§]Computational Biomolecular Dynamics Group, Max Planck Institute for Biophysical Chemistry, 37077 Gottingen, Germany, and [¶]Division of General Zoology, Department of Biology, University of Kaiserslautern, 67653 Kaiserslautern, Germany

Ammonia is a biologically potent molecule, and the regulation of ammonia levels in the mammalian body is, therefore, strictly controlled. The molecular paths of ammonia permeation across plasma membranes remain ill-defined, but the structural similarity of water and NH_3 has pointed to the aquaporins as putative NH_3-permeable pores. Accordingly, a range of aquaporins from mammals, plants, fungi, and protozoans demonstrates ammonia permeability. Aquaporin 4 (AQP4) is highly expressed at perivascular glia end-feet in the mammalian brain and may, with this prominent localization at the blood-brain-interface, participate in the exchange of ammonia, which is required to sustain the glutamate-glutamine cycle. Here we observe that AQP4-expressing *Xenopus* oocytes display a reflection coefficient <1 for NH_4Cl at pH 8.0, at which pH an increased amount of the ammonia occurs in the form of NH_3. Taken together with an NH_4Cl-mediated intracellular alkalization (or lesser acidification) of AQP4-expressing oocytes, these data suggest that NH_3 is able to permeate the pore of AQP4. Exposure to NH_4Cl increased the membrane currents to a similar extent in uninjected oocytes and in oocytes expressing AQP4, indicating that the ionic NH_4^+ did not permeate AQP4. Molecular dynamics simulations revealed partial pore permeation events of NH_3 but not of NH_4^+ and a reduced energy barrier for NH_3 permeation through AQP4 compared with that of a cholesterol-containing lipid bilayer, suggesting AQP4 as a favored transmembrane route for NH_3. Our data propose that AQP4 belongs to the growing list of NH_3-permeable water channels.

Ammonia is an integral constituent in cell metabolism, but its homeostasis is, due to the biological toxicity of ammonia (1–4), highly regulated around 10–35 μM in plasma (5). Ammonia is a base and thus exists in two forms: NH_3 (ammonia) or NH_4^+ (ammonium ion). Henceforward, the term ammonia will be used as a general form, whereas NH_3 and NH_4^+ will be used when referring to a specific form. At physiological pH, its pK_a of 9.25 dictates that ~1.5% of the ammonia is found as NH_3, whereas the rest exists as NH_4^+, the latter of which absolutely requires membrane transporters or channels to cross the plasma membrane. Although dedicated NH_4^+ transport proteins have been identified (6), NH_4^+ is, due to its resemblance to K^+, in addition transported by a range of K^+ transporters and channels, such as the Na^+/K^+-ATPase, the $Na^+/K^+/2Cl^-$ cotransporter, the K^+/Cl^- cotransporter, and inwardly rectifying, voltage-, and Ca^{2+}-activated K^+ channels (7–16). The permeability of NH_4^+ through K^+ channels usually amounts to ~10–20% of the permeability of K^+ (7). It was long believed that NH_3 could permeate the cell membrane by simple diffusion because of its small size and lack of electric charges. NH_3 is, however, a polar molecule with a dipole moment of 1.47 D (close to that of water = 1.85 D; see Fig. 1 for a structural comparison) and may thus permeate poorly through lipid bilayers. Indeed, plasma membranes with poor NH_3 permeability have been demonstrated (17–19), indicating that membrane transport proteins may facilitate NH_3 permeation. The structural similarity of water and NH_3 points to water channels, the aquaporins, as putative NH_3-permeable pores; the plant aquaporins of the tonoplast intrinsic membrane protein (TIP) family, the nodulin-26 like intrinsic protein (NIP) family, and aquaporins from the human-pathogenic protozoans *Plasmodium falciparum*, *Toxoplasma gondii*, and *Trypanosoma brucei* have indeed been shown to allow NH_3 permeation (20–26). The 13 mammalian aquaporins are classified into three families based on their permeability profile and sequence homology: the aquaporins (AQP0, AQP1, AQP2, AQP4,[6] AQP5, AQP6, and AQP8), the aquaglyceroporins (AQP3, AQP7, AQP9, and AQP10), which in addition to water are permeable to small hydrophilic molecules such as urea and glycerol, and the unorthodox aquaporins (AQP11 and AQP12), which share little sequence homology with the other aquaporins (27, 28). Several of both the aquaporins and aquaglyceroporins have been reported to be permeable to ammonia as well as water; AQP1, AQP3, AQP6, AQP7, AQP8, and AQP9 have been found to be permeable for NH_3 (21, 22, 29–31), although the NH_3 permeability of AQP1 has been questioned (21, 22, 32), whereas AQP0, AQP2, AQP5, and AQP4 have been reported to lack NH_3 permeability (29, 31). The sensitivity of the different experimental approaches employed to determine the NH_3 permeability is not defined, and it is possible that, as most K^+

* The authors declare that they have no conflicts of interest with the contents of this article.

[1] Both authors contributed equally.

[2] Supported by the Danish Medical Research Council.
[3] Supported by the Max Planck Society and the German Research Foundation via the SFB 803 (Project A03).
[4] Supported by the Deutsche Forschungsgemeinschaft (DE 231/24-2).

[5] To whom correspondence should be addressed: Dept of Neuroscience and Pharmacology, University of Copenhagen, Blegdamsvej 3, Bldg. 22.3, 2200 Copenhagen N, Denmark. Tel.: 45-35327566; E-mail: macaulay@sund.ku.dk.

[6] The abbreviations used are: AQP4, aquaporin 4; US, umbrella sampling; PMF, potential of mean force; POPC, 1-palmitoyl-2-oleoyl-sn-glycero-3-phosphocholine.

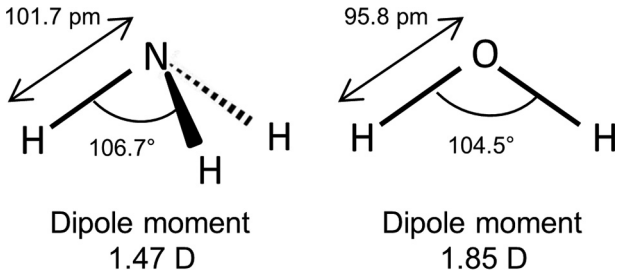

FIGURE 1. **The Lewis structure of NH_3 (*left*) and H_2O (*right*).** NH_3 and H_2O have several similarities including dipole moment (1.47 D for NH_3 and 1.85 for H_2O), tetrahedral electronic structure, bond angle (106.7° for NH_3 and 104.5° for H_2O), and bond length (101.7 pm for NH_3 and 95.8 pm for H_2O).

channels are permeable to NH_4^+, NH_3 permeability may be a general feature in most aquaporins, albeit to a varying degree and, therefore, to a variable degree of detectability. In support of a common water and NH_3 permeability pathway, a H^+-coupled NH_3 co-transporter (SLC4A11) has been demonstrated to allow for water permeation (33, 34).

During acute liver failure, ammonia levels increase in the plasma followed by brain accumulation approaching 5 mM in severe cases (35). This ammonia rise is thought to be the key factor in the pathogenesis of hepatic encephalitis and affects a range of brain functions, *i.e.* cerebral blood flow, cerebral glucose metabolic rate, synaptic transmission, glutamate homeostasis, and cell volume regulation (36–41). However, the paths of ammonia entry into the brain as well as into the cellular compartments of the brain are unresolved. The robust expression of AQP4 at the perivascular glial end-feet surrounding the brain capillaries (42) and the ammonia-dependent regulation of AQP4 membrane expression (43, 44) may suggest AQP4 as a possible entry point of NH_3 into the glial compartments. In the present study, we therefore determine the ammonia permeability of AQP4 by both experimental approaches and molecular dynamics simulations.

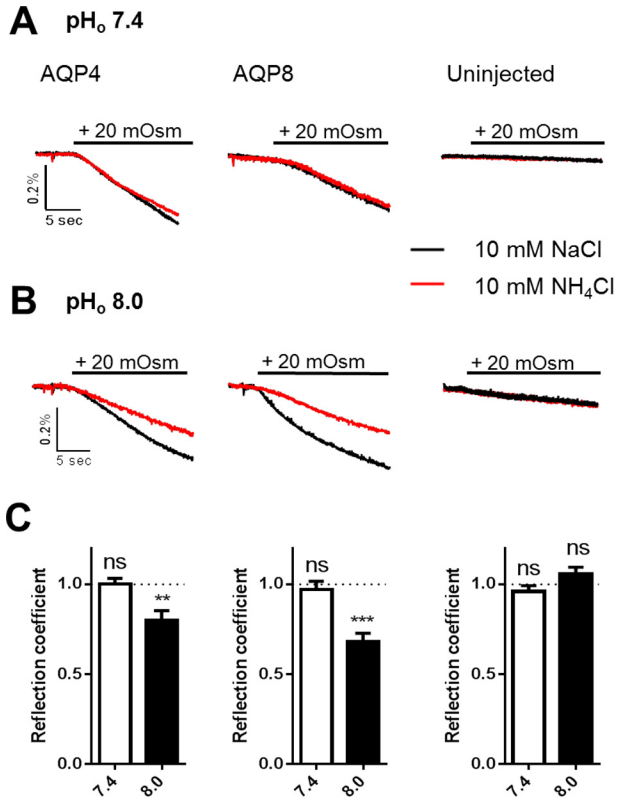

FIGURE 2. **The reflection coefficient is reduced for ammonia in AQP4- and AQP8-expressing oocytes.** *A* and *B*, volume traces from an AQP4-expressing, AQP8-expressing, or uninjected oocyte challenged with a hyperosmotic gradient of 20 mOsM (marked with a *black bar*) of either 10 mM NaCl (*black trace*) or 10 mM NH_4Cl (*red trace*) at pH$_o$ 7.4 (*A*) or pH$_o$ 8.0 (*B*). *C*, A summary of the reflection coefficients for ammonia for AQP4-expressing (*left panel*), AQP8-expressing (*middle panel*), and uninjected oocytes (*right panel*) at pH$_o$ 7.4 and pH$_o$ 8.0. The reflection coefficient is calculated from two control measurements (10 mM NaCl as the osmolyte) and two measurements using 10 mM NH_4Cl as the osmolyte for each oocyte; $n = 7$–12. Statistical significance was determined with paired Student's *t* test. **, $p < 0.01$; ***, $p < 0.001$; *ns*, not significant.

Results

A Low Reflection Coefficient of Ammonia Indicates Ammonia Permeability in AQP4—To determine whether ammonia permeates AQP4, we monitored the ability of ammonia to drive osmotic water flux in *Xenopus* oocytes expressing AQP4 and, as a positive control, the ammonia-permeable AQP8 (22, 31, 45, 46). An inherent advantage in this heterologous expression system is the low intrinsic water permeability of the native oocyte membrane; expression of AQP4 increases the osmotic water permeability of the oocyte membrane ~20-fold (47, 48), thus providing a robust signal-to-noise ratio. AQP4- and AQP8-expressing oocytes exposed to an osmotic challenge consisting of the impermeable osmolyte NaCl (10 mM; 20 mOsM) therefore, as opposed to uninjected oocytes, displayed robust cell shrinkage (water permeabilities at pH 7.4 in $\times 10^{-3}$ cm/s: 2.99 ± 0.49, $n = 12$ for AQP4, 2.04 ± 0.39, $n = 9$ for AQP8, and 0.14 ± 0.01, $n = 7$ for uninjected oocytes, $p < 0.05$ for both AQP4 and AQP8 when compared with uninjected); see the representative traces in *black* in Fig. 2*A*. To obtain the reflection coefficient of ammonia, the same oocytes were then exposed to an identical osmotic challenge of 20 mOsM but obtained with NH_4Cl (10 mM) as the osmolyte. Both oocytes expressing AQP4 and AQP8 as well as uninjected oocytes responded to the osmotic challenge in a manner essentially identical to that observed with NaCl as the osmolyte (water permeabilities with NH_4Cl as the osmolyte in $\times 10^{-3}$ cm/s: 3.04 ± 0.42, $n = 12$ for AQP4, 1.94 ± 0.37, $n = 9$ for AQP8, and 0.13 ± 0.01, $n = 7$ for uninjected oocytes, $p < 0.05$ for both AQP4 and AQP8 when compared with uninjected); see the representative traces in *red* in Fig. 2*A*. The reflection coefficient for ammonia at pH 7.4, $\sigma_{7.4}$, was therefore not significantly different from 1 (1.00 ± 0.03, $n = 12$ for AQP4, 0.96 ± 0.04, $n = 9$ for AQP8, and 0.96 ± 0.03, $n = 7$ for uninjected oocytes), illustrated as *white bars* in Fig. 2*C*. Of the 10 mM NH_4Cl, only 0.14 mM exists as NH_3 at pH 7.4 and the reminder exists as NH_4^+ (according to the Henderson-Hasselbalch equation). To increase the fraction of NH_3 in the test solution without changing the ammonia concentration, a parallel experimental series was carried out with test solutions of pH 8.0, in which the NH_3 concentration is 4-fold higher (0.56 mM). The slightly basic test solutions did not significantly affect the water permeability obtained with NaCl as the osmolyte (water permeabilities at pH 8.0 in $\times 10^{-3}$ cm/s: 2.34 ± 0.28 $n = 12$ for AQP4, 1.16 ± 0.25, $n = 9$ for AQP8, and 0.23 ± 0.04, $n = 7$ for uninjected oocytes); see the representative traces in *black*

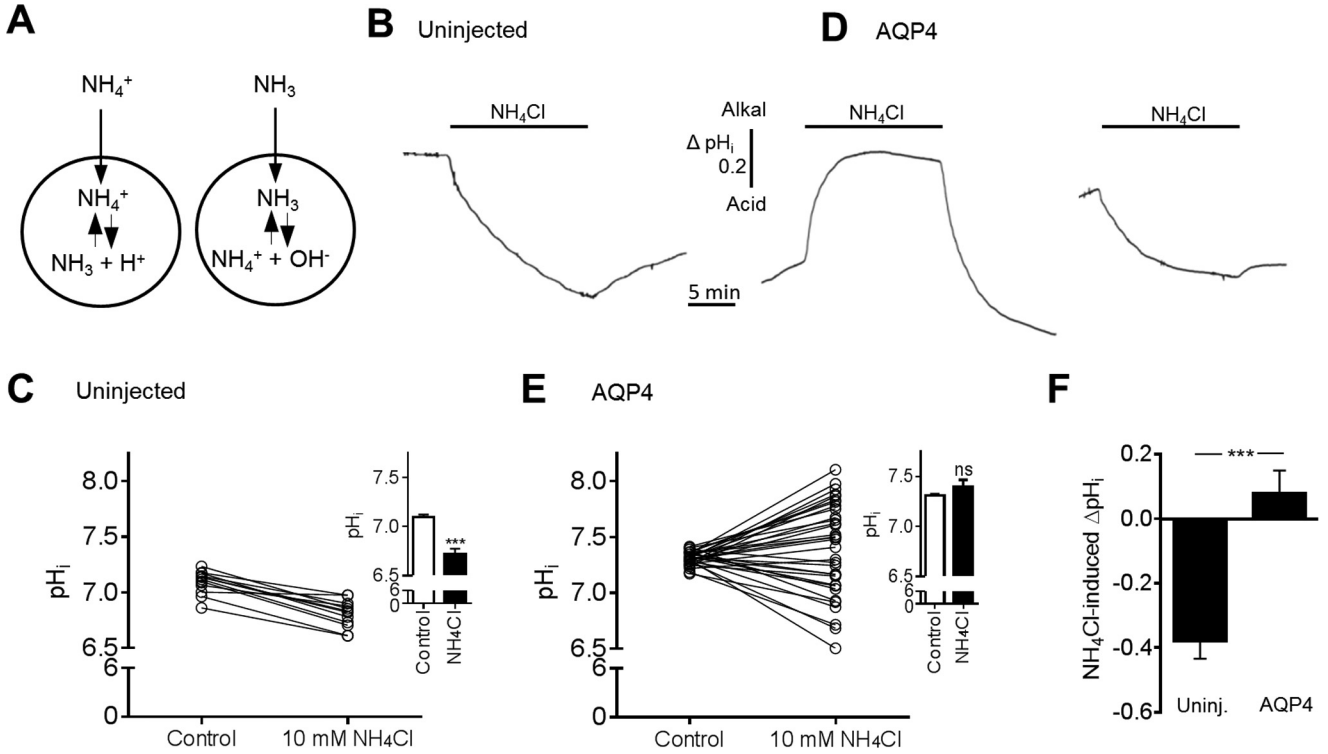

FIGURE 3. **pH_i changes in response to exposure to ammonia in uninjected and in AQP4-expressing oocytes.** *A*, transport of ammonia as either NH_4^+ or NH_3. If NH_4^+ crosses the cell membrane, it will cause an intracellular acidification, whereas influx of NH_3 will cause an intracellular alkalization. *B* and *D*, pH_i traces from an uninjected oocyte (*B*) and from two AQP4-expressing oocytes (*D*) exposed to 10 mM NH_4Cl (marked with a *black bar*). *C*, overview of the individual pH_i changes in uninjected oocytes after 15 min of exposure to 10 mM NH_4Cl, summarized in the *inset*, $n = 15$. *E*, overview of the individual pH_i changes in AQP4-expressing oocytes after 15 min of exposure to 10 mM NH_4Cl, summarized in the *inset*, $n = 33$. *F*, overview of the NH_4Cl-induced ΔpH_i in uninjected (*Uninj.*) oocytes ($n = 15$) and AQP4-expressing oocytes ($n = 33$). Statistical significance was determined with paired Student's *t* test (unpaired Student's *t* test in *panel F*). ***, $p < 0.001$; *ns*, not significant.

in Fig. 2*B*. These results demonstrate that the higher pH of the extracellular solution in itself did not affect the water permeability of either the AQPs or the native plasma membrane. An osmotic challenge based on NH_4Cl (at pH 8.0) provided a cell shrinkage of the uninjected oocytes identical to that obtained with NaCl; see the *red trace* in Fig. 2*B*, *right panel*, for a representative trace. Oppositely, the osmotic water permeability was significantly smaller for both AQP4- and AQP8-expressing oocytes when obtained with NH_4Cl instead of NaCl; see the *red traces* in Fig. 2*B*, *left* and *middle panels*, for representative traces. The reflection coefficient for NH_4Cl at pH 8, $\sigma_{8.0}$, was, therefore, significantly <1 for the AQP-expressing oocytes (0.80 ± 0.05, $n = 12$ for AQP4, $p < 0.01$ and 0.68 ± 0.04, $n = 9$ for AQP8, $p < 0.001$), whereas for the uninjected oocytes, $\sigma_{8.0}$ was not significantly different from 1 (1.07 ± 0.04, $n = 8$), summarized as *black bars* in Fig. 2*C*. These data suggest that at pH 8.0, at which the test solutions contain a significant NH_3 content, we detect ammonia permeation into the pore of the expressed aquaporins, thus preventing ammonia from exerting the full osmotic force as observed with the impermeable NaCl.

AQP4 Alters the pH_i Response to Ammonia Treatment of Oocytes—Cellular influx of NH_3 causes intracellular alkalinization, whereas NH_4^+ influx causes intracellular acidification, as illustrated in Fig. 3*A*. To further resolve the ability of ammonia to permeate AQP4, we monitored the intracellular pH of uninjected and AQP4-expressing oocytes with a H^+-sensitive microelectrode during the addition of ammonia to the extracellular solution. A stable pH_i baseline was obtained in control solution before exposure of the oocytes to an isosmotic solution containing 10 mM NH_4Cl for 15 min. NH_4Cl caused an intracellular acidification of all uninjected oocytes (representative trace in Fig. 3*B* and summarized data in Fig. 3*C*; compare pH_i of 7.10 ± 0.02 in control solution with 6.72 ± 0.06 in the presence of ammonia, $n = 15$, $p < 0.001$, *inset*). AQP4-expressing oocytes responded in a graded manner with the majority of the tested oocytes responding to NH_4Cl with either a robust intracellular alkalization or a lesser acidification than observed with the uninjected oocytes (representative traces are illustrated in Fig. 3*D*; summarized data are in Fig. 3*E*, $n = 33$). 6 of the 33 tested oocytes responded with a pH_i change that fell within the confidence interval of the pH_i change observed in the uninjected oocytes (ΔpH_i of −0.38 (CI −0.49 to −0.26) pH units, $n = 15$). Summarized data illustrate that the intracellular acidification observed in uninjected oocytes was abolished in the AQP4-expression oocytes; compare pH_i of 7.31 ± 0.01 in control solution with 7.39 ± 0.07 in NH_4Cl-containing solution, $n = 33$, $p = 0.26$, Fig. 3*E*, *inset*. The NH_4Cl-induced pH_i change in AQP4-expressing oocytes (0.08 ± 0.07 pH units, $n = 33$) was thus significantly different from that obtained in uninjected oocytes (-0.38 ± 0.06 pH units, $n = 15$), $p < 0.001$, Fig. 3*F*. The observed alkalization (or lesser acidification) in a substantial fraction of the AQP4-expressing oocytes (27/33),

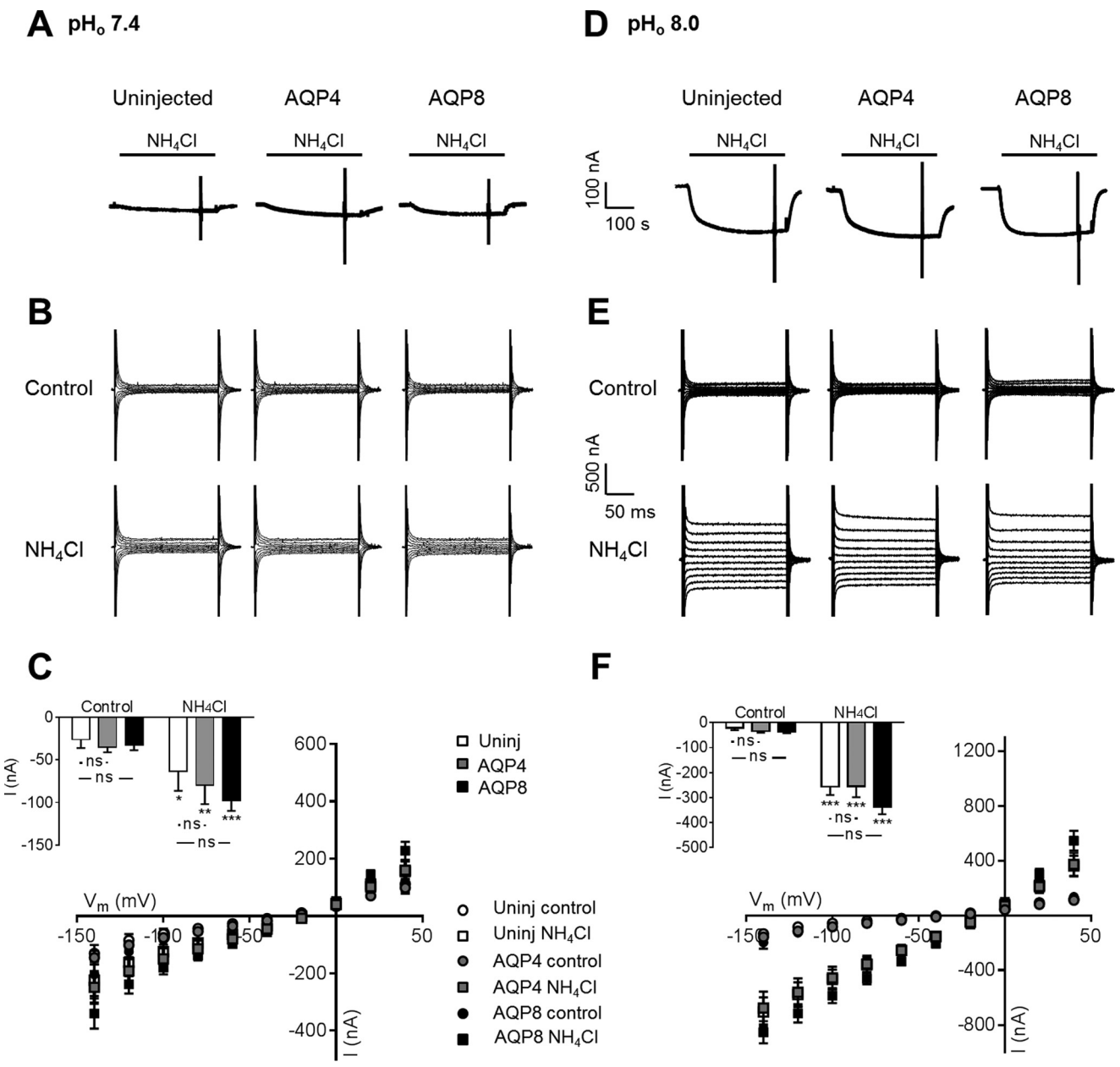

FIGURE 4. **No aquaporin-mediated NH_4^+ permeation.** *A* and *D*, representative current traces in uninjected (*left panel*), AQP4 (*middle panel*)-, and AQP8 (*right panel*)-expressing oocytes at pH_o 7.4 (*A*) and pH_o 8.0 (*D*) before and in the presence of 5 mM NH_4Cl, marked with a *black bar*. The currents were recorded from single oocytes at a holding potential of −50 mV. *B* and *E*, representative *I/V* relationships of uninjected (*left panels*), AQP4 (*middle panels*)-, or AQP8 (*right panels*)-expressing oocytes at pH_o 7.4 (*B*) and pH_o 8.0 (*E*) before and after 5 min of treatment with 5 mM NH_4Cl. *C* and *F*, summarized *I/V* relationships of uninjected (*Uninj.*) oocytes (*white*) and oocytes expressing AQP4 (*gray*) or AQP8 (*black*) before and after treatment with 5 mM NH_4Cl at pH_o 7.4 (*C*) and pH_o 8.0 (*F*), $n = 9$ of each, with the currents obtained at $V_m = -60$ mV summarized in the *insets*. Statistical significance was determined with two-way analysis of variance with Šídák's multiple comparison post hoc test. *, $p < 0.05$; **, $p < 0.01$; ***, $p < 0.001$; *ns*, not significant.

therefore, suggests that ammonia is able to permeate the pore of AQP4 in the form of NH_3.

Expression of AQP4 Does Not Induce NH_3/NH_4^+-dependent Membrane Current in Oocytes—To determine if AQP4 was permeable to NH_4^+, we monitored the current response of uninjected oocytes and AQP4- and AQP8-expressing oocytes during ammonia exposure. NH_4^+ membrane permeation results in a membrane current in voltage clamped oocytes which is absent with NH_3 permeation. At pH 7.4, isosmotic addition of 5 mM NH_4Cl to the test solution caused a small inward current in both uninjected oocytes and AQP-expressing oocytes; see the representative current traces in Fig. 4*A*. Voltage step protocols applied before and after the addition of ammonia illustrated comparable membrane currents in uninjected oocytes and AQP4- and AQP8-expressing oocytes both in control solution and after exposure to ammonia (see representative *I/V* current traces in Fig. 4*B*, summarized *I/V* relations in Fig. 4*C*, and summarized currents at −60 mV displayed as the inset); although the membrane current increased in the presence of ammonia for all tested oocytes (uninjected oocytes: compare −26.3 ± 9.9 nA with −63.7 ± 22.7 nA in the presence of ammonia, $n = 9$, $p < 0.05$; AQP4: compare −35.1 ± 6.0 nA with −79.9 ± 22.1

nA in the presence of ammonia, $n = 9$, $p < 0.05$; AQP8: compare -32.7 ± 6.0 nA with -97.5 ± 12.4 nA in the presence of ammonia, $n = 9$, $p < 0.001$), the increase observed in the AQP-expressing oocytes was not significantly different from that of the uninjected oocytes; see the Fig. 4*C inset*. To obtain an increased fractional NH_3 content, a parallel experimental series was carried out at pH_o 8.0. Although the ammonia-induced membrane currents intrinsic to the native oocyte membrane was enlarged at this extracellular alkalinization, the observed current pattern resembled that obtained at pH_o 7.4; see the representative current traces in Fig. 4*D*, representative *I*/*V* current traces in Fig. 4*E*, and the summarized *I*/*V* relations in Fig. 4*F* with an *inset* summarizing the current obtained at $V_m = -60$ mV (uninjected: compare -21.8 ± 8.0 nA with -256.4 ± 32.9 nA in the presence of ammonia, $n = 9$, $p < 0.05$; AQP4: compare -35.0 ± 5.5 nA with -255.7 ± 42.4 nA in the presence of ammonia, $n = 9$, $p < 0.05$; AQP8: compare -35.7 ± 6.4 nA with -336.3 ± 29.5 nA in the presence of ammonia, $n = 9$, $p < 0.001$). At pH_o 8.0 as well as pH_o 7.4, the ammonia-induced membrane currents were independent of aquaporin expression in the plasma membrane, which supports that AQP4- and AQP8-dependent ammonia permeation takes place via NH_3 rather than via NH_4^+.

Partial Ammonia Permeation Was Observed in Free Simulations—To obtain details on ammonia entry into the pore of AQP4 on a molecular scale, we performed molecular dynamics on this permeability event. Free simulations were initially carried out to observe the behavior of both NH_3 and NH_4^+ near the surface of AQP4. In these simulations we introduced, separately, 100 molecules each of NH_3 and NH_4^+ with appropriate neutralization for the latter. Each simulation was carried out for 500 ns. For any further analysis, only the latter 400 ns were considered to account for equilibration effects. We observed several partial permeation events of NH_3 entering the channel and exiting from the same end. Together, these partial permeation events cover almost the entire protein pore. In contrast, NH_4^+ never penetrated the pore to any significant extent. Remarkably, NH_4^+ showed high propensity to cluster around several anionic amino acids such as glutamate and aspartate on either protein surface (Fig. 5). Most of these clustering "hotspots" are placed closely to the opening of the channel pore.

The Free Energy Barrier for NH_3 Permeation through AQP4 Is Surmountable but Higher Than for Water Permeation—To determine the free energy profiles of NH_3 permeation via AQP4 *versus* via lipid membranes of different composition, we carried out umbrella sampling (US) simulations, in which we calculated the potential of mean force (PMF) for NH_3 permeation through the pore of AQP4. The uncertainty in the PMF calculation was ascertained using a bootstrapping algorithm as implemented in the g_wham tool from GROMACS and is illustrated as a *shaded margin around the PMF curves*, see Fig. 6*A*. The radius profile for the channel is shown for reference in Fig. 6*B*. To gauge the permeability of AQP4 to NH_3, we compared these PMFs to free energy profiles calculated across lipid bilayers. We used two lipid membranes for comparison; a pure 1-palmitoyl-2-oleoyl-sn-glycero-3-phosphocholine (POPC) bilayer and a hybrid bilayer with 20% cholesterol and 80% POPC. This latter comparison is shown in Fig. 6*A*. The free energy barrier for NH_3 permeation through AQP4 is comparable with that of the POPC pure membrane, whereas the barrier is ~3–4 kJ/mol lower in the AQP4 pore than in the lipid membrane containing 20% cholesterol. These results suggest that the free energy barrier of NH_3 permeation may indeed favor permeation through AQP4 rather than through a cholesterol-containing lipid membrane. The radius profile shown in Fig. 6*B* allows us to understand where the channel is narrowest. This can contribute to the entropic barrier for entering the channel and also to the overall loss of the hydrogen bonding from water as hydration of the NH_3 decreases in a narrow region of the channel. In addition to the channel pore profile, the pore-lining residues are illustrated in Fig. 6*C* as a histogram of their position along the *z* axis. These residues could potentially supplement the hydrogen bonding to the NH_3 depleted from the lack of hydration.

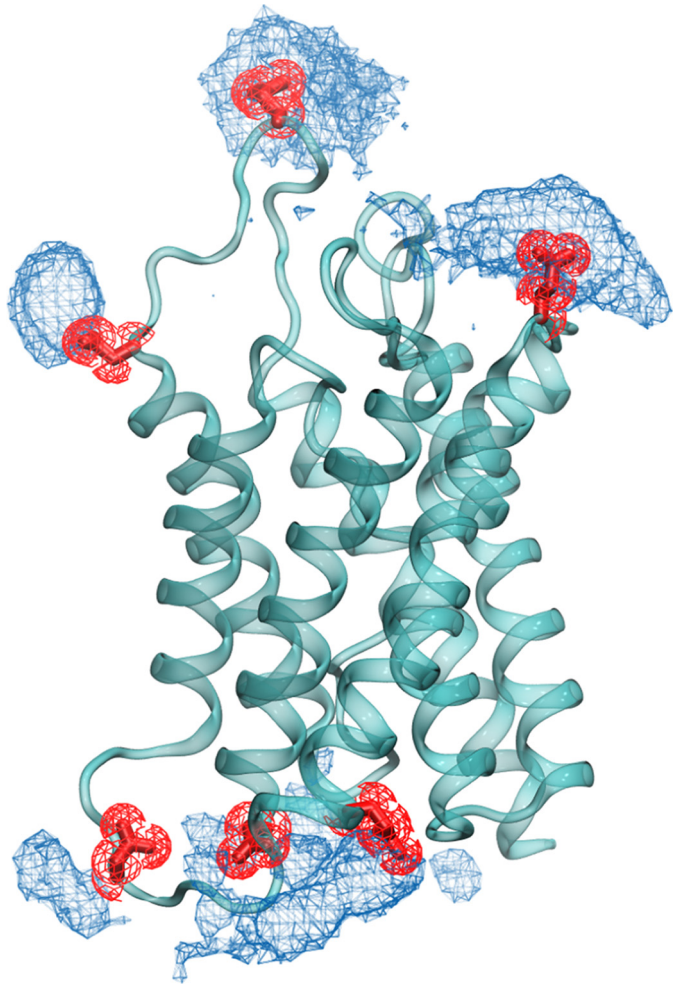

FIGURE 5. **Accumulation of NH_4^+ close to the channel surface.** In free simulations the NH_4^+ density (illustrated as *blue mesh*) is placed closely to the glutamate and aspartate residues on the protein surface, shown in *red licorice representation*.

To compare the free energy barrier for NH_3 with that of water, we performed free simulations in the absence of NH_3 or NH_4^+ and calculated the PMF for water across AQP4 (Fig. 7*A*). The uncertainty in the PMF for these simulations is represented by the standard deviation of the PMF along the four monomers and illustrated as a *shaded margin around*

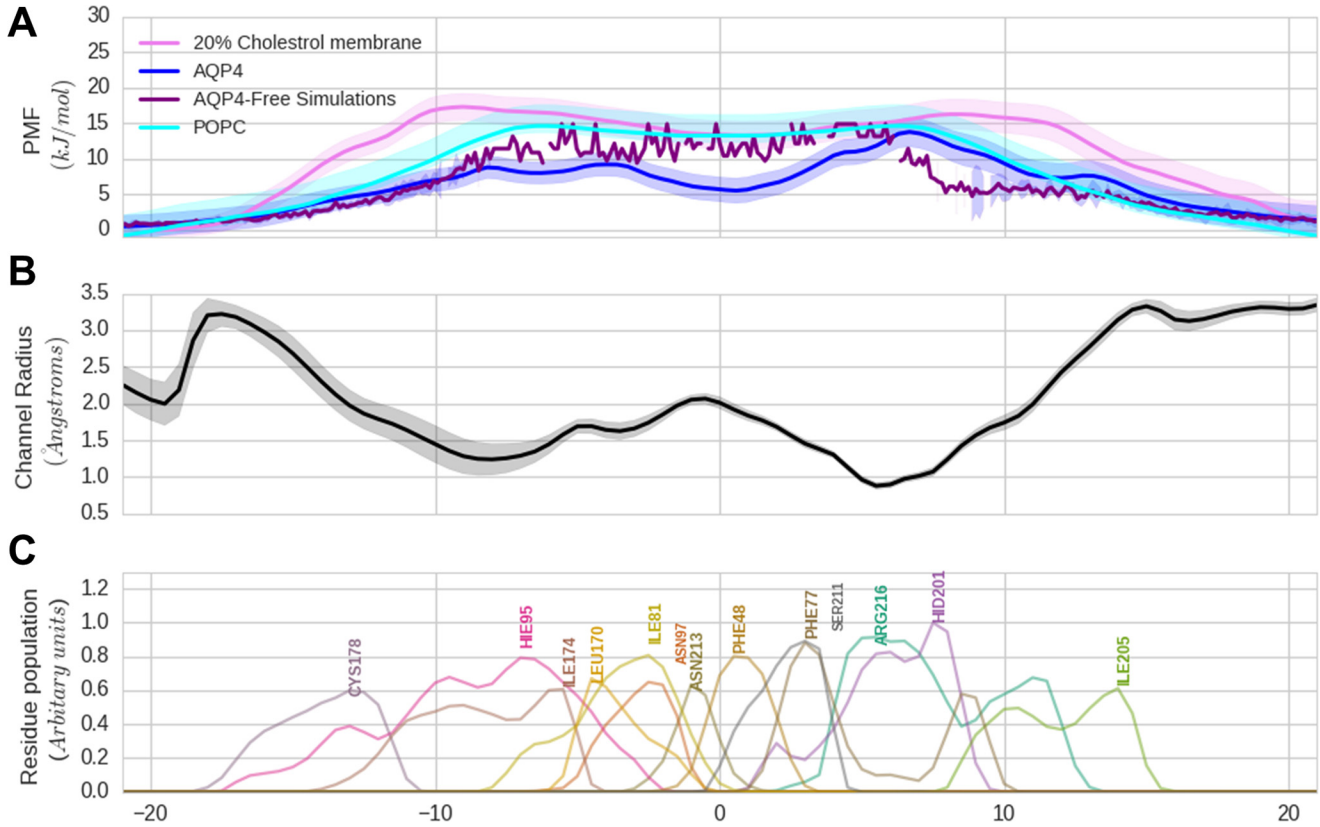

FIGURE 6. Potential of mean force for NH_3 permeation (*A*). Shown is a comparison of the PMF for NH_3 through the AQP4 channel with the membrane. The PMF of NH_3 through AQP4 is shown in *blue*. The PMF for NH_3 through a pure POPC lipid bilayer is shown in *cyan*. The PMF for NH_3 through a lipid bilayer with 20% cholesterol is shown in *purple*. The uncertainty measured via bootstrapping is shown in the *shaded region around the curves*. The *broken violet curve* is the PMF for NH_3 through AQP4 extracted from the free simulations. *B*, radius profile of the AQP4 pore along the channel axis. The *shaded region* represents the standard deviation in the profile over the simulation trajectory. *C*, population histogram of the important pore lining residues along the channel axis.

the PMF curve in Fig. 7*A*. The differences in the free energy profile for NH_3 compared with water are illustrated as a *hatched region* in Fig. 7*A* and points to the fact that water is preferred to ammonia for channel entry along almost the entire channel axis. To understand the origin of contribution of protein-NH_3 and NH_3-water hydrogen bonding to the PMF, we calculated the average number of hydrogen bonds of NH_3 with pore-lining amino acid residues from the US windows (Fig. 7*B*). The overall loss of hydrogen-bonding energy for the system as a whole observed when NH_3 enters the channel, by convention a positive number, is shown in Fig. 7*C*. This loss is quantified by use of the US windows by comparing the total hydrogen-bonding energy of a water-filled AQP4 pore against a pore in which NH_3 was introduced. For calculating the hydrogen-bonding energy of the water-filled pore, we took into account the protein and the 30 water molecules nearest to the channel center. We found that these consistently accounted for all the hydration inside the channel pore. The choice of this smaller number allowed us to minimize the fluctuations in the evaluation of hydrogen bonding energy. In the case of the US simulation windows, we chose only the first 29 water molecules to account for the presence of NH_3, which sterically replaces approximately one water molecule in the pore. An average over the trajectories in each window was used to calculate the mean difference in the hydrogen-bonding energy, and the standard error indicated the uncertainty in the estimation of the difference in energy thus obtained.

Discussion

In the present study we observed an ability of NH_3, but not NH_4^+, to gain access to the pore of AQP4 in a manner suggesting that AQP4 may belong to the growing number of aquaporins acting as NH_3 channels. The permeation of small hydrophobic molecules such as CO_2 or O_2 is expected to take place via passive diffusion across the lipid bilayer. In contrast, charged or polar molecules such as ions or water require a dedicated channel for their optimal conduction across the membrane. NH_3 presents an intriguing intermediate case with a capacity for hydrogen-bonding and low polarity. Thus, deciphering the permeation path of NH_3 across the lipid bilayer requires further study. Hub *et al.* (49) have shown that NH_3 experiences a low barrier (~6 kT or about 14 kJ/mol) for its passage across pure lipid membranes such as those composed of phosphatidylethanolamine or phosphocholine lipids. However, pure lipid membranes are generally only present in synthetic setups and do not represent a physiological situation. Biological membranes are often complex assemblies made up of several lipid types and sterols. Animal membranes, in particular, are rich in cholesterol, which can drastically alter the permeation properties of small molecules. Additionally, the cell membrane may be obstructed for entry due to high concentration of proteins or

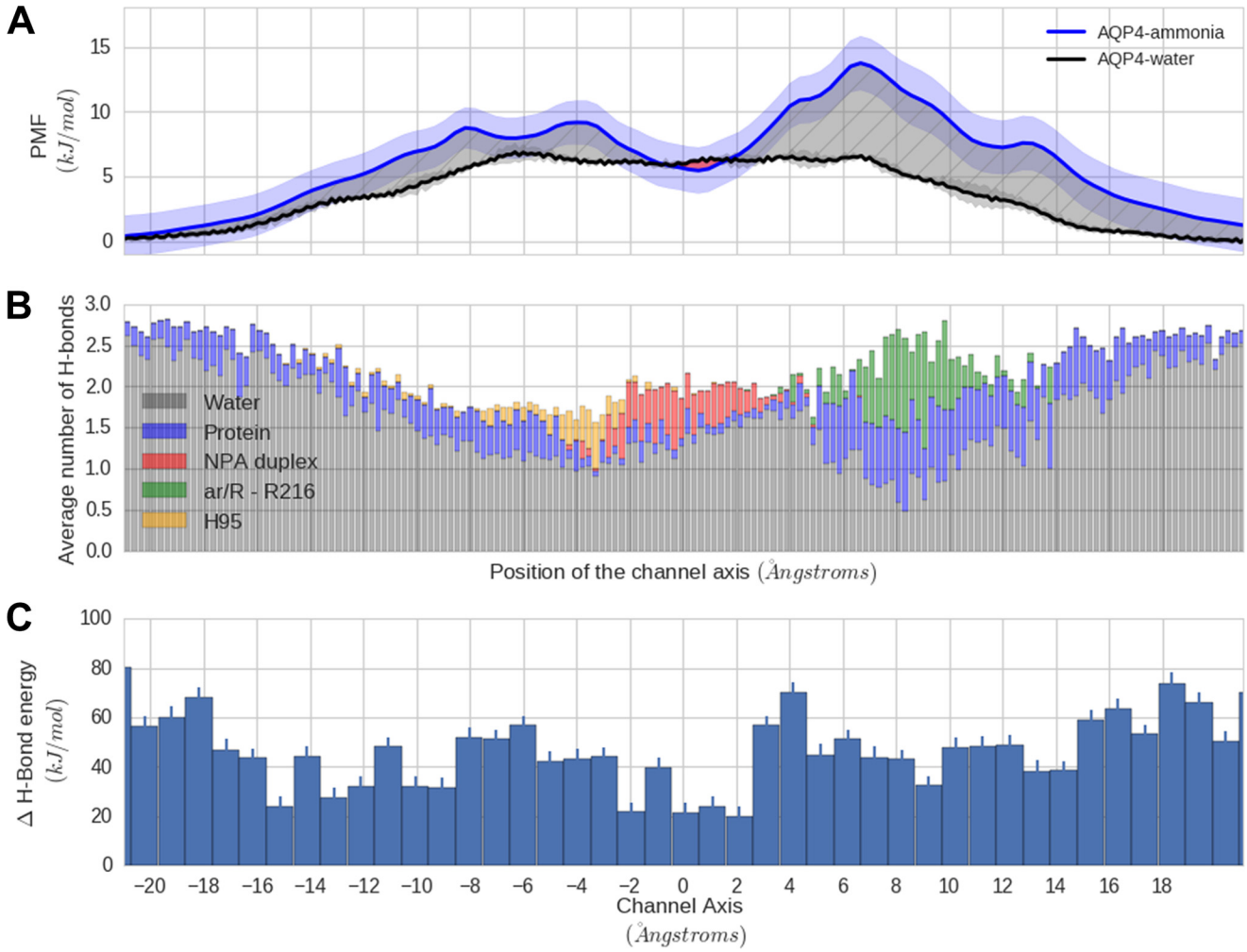

FIGURE 7. **Comparison of water and NH$_3$ permeation in AQP4.** *A*, NH$_3$ has a significantly larger (~5 kJ/mol) free energy barrier over water in AQP4 calculated from free simulations. *B*, as NH$_3$ loses hydration via hydrogen bonding on its entry into the channel, the average number of hydrogen bonds to the channel axis. *C*, hydrogen bonding energy (*HBE*) difference for water and NH$_3$ along the channel axis ($HBE_{NH3} - HBE_{water}$). The positive difference indicates that hydrogen bonding with water is favored in the channel.

even because of glycosylation of lipids or protein covering the membrane surface. This might make an otherwise convenient means of diffusive passage less accessible. Thus, it might be necessary to take into account alternative means available for NH$_3$ conductance. Sometimes, these alternative routes might be as or more effective than passive membrane diffusion. Aquaporins have been long speculated to be involved in gas transport across cell membranes, and a range of aquaporins from plants, protozans, and mammals have been demonstrated to share the ability of NH$_3$ permeation in addition to their intrinsic water permeability (20–26, 29–31, 46, 50). Our experimental data show NH$_3$ permeation through AQP4 expressed in *Xenopus* oocytes measured as a reduced reflection coefficient of NH_4Cl and as the ability of NH_4Cl to promote intracellular alkalinization of AQP4-expressing oocytes. A low reflection coefficient ($\sigma < 1$) suggests that the osmolyte in question gains access to the aqueous pore and, therefore, is unable to osmotically extract water from the cell as efficiently as that of a non-permeable (reflected) osmolyte. We were, however, unable to detect a reduced reflection coefficient at pH 7.4, at which the NH$_3$ content in our 10 mM NH_4Cl-containing test solution was exceedingly low. At pH 8.0, the NH$_3$ fraction was calculated to reach 0.56 mM, and under these conditions oocytes expressing either AQP4 or AQP8 (a well established NH$_3$ channel (Refs. 22, 31, 45, and 46)) both displayed a lower osmotic water permeability with NH_4Cl as the osmolyte. The water permeability of the native oocyte membrane was unaffected by the choice of osmolyte and pH_o, indicating that the observed changes in water permeability originated in the expressed AQPs and suggests NH$_3$ permeation through both AQP4 and AQP8. Exposure of uninjected oocytes to NH_4Cl persistently caused an intracellular acidification, as previously observed (22, 30, 51–54), which is assigned to NH_4^+ entry through still unidentified pathways, presumably cation-selective ion channels (53, 55). Although a small fraction of the AQP4-microinjected oocytes displayed a similar acidification, the majority of the tested AQP4-expressing oocytes displayed either a lesser acidification or a robust alkalization upon exposure to ammonia with no obvious correlation to initial pH_i or days in culture. We, therefore, cannot explain the graded response in these oocytes, which was also observed in AQP1-expressing oocytes (30). The exact placement of the electrode tip could affect the extent of

detection of a given pH_i change, and different levels of AQP4 expression in the tested oocytes likely affects the level of alkalization (functional AQP4 expression was tested for all oocytes by a simple, non-quantitative swelling assay that reveals the presence of an aquaporin in the oocyte membrane but not its abundance). This alkalization (or lesser acidification) suggests the ability of AQP4 to allow permeation of NH_3. The observed AQP4-mediated NH_3 permeation is at odds with previous reports by Boron and co-workers (29, 31) who were unable to demonstrate NH_3 permeability in AQP4-expressing oocytes. In those studies, NH_3 permeation was evaluated by monitoring the pH_o at the external face of the oocyte plasma membrane with a blunt microelectrode pushed against the surface of an AQP-expressing oocyte. A reason for the discrepancy with our result may rely on the 20-fold difference in applied NH_4Cl (0.5 mM in Refs. 29 and 31) *versus* 10 mM in this study. At the low NH_4Cl concentration employed by Boron and co-workers (29, 31), only 0.007 mM exists as NH_3 and in case AQP4 has a lower NH_3 permeability capacity than the other tested aquaporins, it may simply be experimentally undetectable at this concentration.

Exposing oocytes to NH_4Cl increased the transmembrane currents, irrespective of the presence of an aquaporin in the plasma membrane, by as yet unidentified pathways (52). We detected, however, no significant difference between the currents obtained in AQP4-expressing oocytes and uninjected oocytes at either of the tested pH values, indicating a lack of NH_4^+ permeation through AQP4. There was a tendency (although statistical significance was not reached in the present study) for the ammonia-induced transmembrane current to be slightly increased in the AQP8-expressing oocytes compared with that of the uninjected oocytes, as previously observed in oocytes expressing AQP8 and other ammonia-permeable aquaporins (22, 26, 32).

To shed light on the thermodynamic parameters that govern the NH_3 permeation in AQP4, we employed molecular simulations. US simulations show that the free energy barrier of ~14 kJ/mol (~6 kT) for NH_3 permeation through AQP4 is surmountable at room temperature. At higher temperatures such as at 37 °C, the attempt rate could encourage the permeation even further. The magnitude of this barrier is comparable with the one associated with a POPC lipid bilayer. Interestingly, the addition of cholesterol to this lipid makes the barrier rise up to ~20 kJ/mol, which is ~5 kJ/mol larger than the free energy barrier for AQP4. The permeation barrier increase observed upon the addition of cholesterol is to be expected, as cholesterol has a tendency to "thicken" the membrane by ordering the lipid tails and closing the small gaps in lipid tails that facilitate diffusion of the gas (49). This might have a real physiological effect *in vivo*, making the AQP4, rather than the plasma membrane, a favored route for NH_3 permeation. Also, 20% cholesterol is a lower limit of the sterol portion in the membrane, and an increased percentage could, therefore, lead to an even further increase in the relative passage of NH_3 through AQP4. In the sub-microsecond time scale employed for the free simulations, we observed partial permeation events of NH_3 through AQP4 that together span almost the complete AQP4 pore. The free simulations are hampered by the potential lack of sampling of putative permeation events due to the finite simulation time. Spontaneous barrier crossing in an unbiased, "free" MD simulation is a stochastic event that may or may not happen in a finite simulation time. Therefore, we took the more systematic approach of US that computes the energetic profile for solute permeation. The US method, due to the enforcement on the coordinate of ammonia across the permeation pathway, ensures that the relevant thermodynamic information concerning permeation is recovered. The barrier of ~14 kJ/mol (6 kT) observed using this method is surmountable under physiological conditions, indicating that the channel is a viable means of permeation. Indeed, the statistics collected from several partial entries of ammonia in the channel allowed us to compare the PMF calculated from the US method to the PMF from the partial permeations (Fig. 6*A*). The barrier, as calculated by the two methods, is remarkably similar, further strengthening the hypothesis that ammonia permeates the channel by diffusion. Thus, overall, the molecular dynamics simulations support the permeation of ammonia across AQP4 at physiological conditions as compared with the lipid bilayer, especially in a lipid environment rich in cholesterol.

AQP4 seems to facilitate the transport of NH_3 by stabilizing the molecule in the channel pore. In the highly conserved and narrow aromatic/arginine (ar/R) region of the protein, we observe several stabilizing hydrogen bonding interactions that seem to partially replace the loss of hydration for NH_3. However, this dehydration appears quite significant (~5 kJ/mol) and seems to be contributed due to a lack of replacement of the hydrogen bonding in the channel compared with the bulk. This "hydrophobic" effect seems to underlie the favored permeation of water over NH_3 through AQP4, as was previously reported to be the main permeation barrier for apolar gas molecules such as O_2 and CO_2 (56). The only region where the PMF for ammonia dips below the PMF for water is close to the asparagine-proline-alanine (NPA) duplex. This dip can be explained based on the enthalpic contribution of hydrogen bonding to the total free energy. We observe that in this region difference in enthalpy of hydrogen bonding of water compared with NH_3 reaches its minimum. Additionally, AQP4 seems to provide a platform for attracting NH_4^+ due to the preponderance of the acidic amino acids that decorate its either face. Speculatively, this could be a potential mechanism to facilitate the conversion of excess NH_4^+ into NH_3. The presence of the negatively charged surface amino acids could thus be of physiological relevance, as these residues could be catalytic sites for accelerating the rate of both forward and backward conversion of NH_3 to NH_4^+ and hence lead to a locally enhanced concentration of NH_3.

NH_4^+ is readily transported by a range of K^+ transporting mechanisms (7–16), whereas NH_3, probably due to its resemblance to water, appears to cross cell membranes by facilitated diffusion through a range of aquaporins, among which we here propose that AQP4 is featured. The cerebral glutamate-glutamine cycle encompasses vesicular release of glutamate from the presynapse with subsequent astrocytic uptake, amidation of glutamate to glutamine (a process requiring free ammonia), shuttling of glutamine to the neuronal structures, and its hydrolyzation to glutamate and ammonia. Due to the toxic property of ammonia, operation of the glutamate-glutamine cycle thus requires that astrocytes exhibit an efficient way of accumulat-

ing and removing ammonia (57). AQP4 is robustly expressed at the perivascular glial end-feet and covers ~50% of the surface area of this membrane (42, 58). It may, with this prime location at the interface between the brain and the blood, participate in facilitation of NH_3 permeation across the glial membrane both under physiological conditions and during hyperammonemia. Hyperammonemia occurs in association with various pathologies, among these acute liver failure, and associates with metabolic alkalosis (59). Increased plasma ammonia levels in combination with alkaline pH will thus, in combination, increase the fraction of ammonia existing as NH_3 and, therefore, even further enhance the AQP4-mediated brain accumulation of ammonia that is consistently observed during hepatic encephalopathy (35). AQP4 may, therefore, be a potential pharmaceutical target in the attempt to limit brain ammonia accumulation during hepatic encephalopathy.

Experimental Procedures

Molecular Biology—Rat AQP4.M23 and rat AQP8 was subcloned into the oocyte expression vector pXOOM, linearized downstream from the poly-A segment, and *in vitro* transcribed using T7 mMessage Machine (Ambion, Austin, TX) according to the manufacturer's instructions. MEGAclear (Ambion) was used to extract the cRNA before micro-injection into defolliculated *Xenopus laevis* oocytes.

Oocyte Preparation—X. laevis frogs were obtained from Nasco (Fort Atkinson, WI) or Xenopus Express (Le Bourg, Vernassal, France). All animal protocols comply with the European Community guidelines for the use of experimental animals, and were approved and performed under a license issued for the use of experimental animals by the Danish Ministry of Justice (Dyreforsøgstilsynet) or by The Landesuntersuchungsamt Rheinland-Pfalz (Koblenz, Germany). Oocytes were surgically removed, and their follicular membrane was removed by incubation in Kulori medium (90 mM NaCl, 1 mM KCl, 1 mM $CaCl_2$, 1 mM $MgCl_2$, 5 mM HEPES, pH 7.4) containing 10 mg/ml collagenase (Type 1, Worthington, Lakewood, NJ) and 1 mg/ml trypsin inhibitor (Sigma) as previously described (48). The oocytes were kept in Kulori medium at 18 °C to recover until the following day, at which time they were microinjected with cRNA encoding AQP4 or AQP8 (25 ng RNA/oocyte) and left at 18 °C for 3–5 days before experiments. All oocyte experiments were performed at room temperature.

Oocyte Volume Measurements—The experimental setup for measuring water permeability of oocytes has been described in detail previously (60). Briefly, the oocyte was placed in a small chamber with a glass bottom and perfused with a control solution at room temperature (95 mM NaCl, 2 mM KCl, 1 mM $CaCl_2$, 1 mM $MgCl_2$, 10 mM HEPES, 5 mM choline chloride, pH 7.4 or pH 8.0). The oocyte was viewed from below via a long distance objective, and oocyte images were captured continuously at a rate of 25 images/s. To determine the water permeability, the oocytes were challenged with a hyperosmotic solution (control solution containing either additional 20 mosM NaCl (10 mM) or 20 mosM NH_4Cl (10 mM)), osmolarities of all solutions verified with an accuracy of 1 mosM with an osmometer Type 15 (Löser Messtechnik, Berlin, Germany), and the water permeability was calculated as,

$$L_p = \frac{-J_v}{A \cdot \Delta\pi \cdot V_w} \quad \text{(Eq. 1)}$$

where Jv is the water flux during the osmotic challenge, A is the true membrane surface area (about nine times the apparent area due to membrane folding (Ref. 61), $\Delta\pi$ is the osmotic challenge, V_w is the partial molal volume of water (18 cm^3/mol), and L_p is the water permeability given in units of (cm/s).

The reflection coefficient for NH_4^+/NH_3, as previously described (22), was calculated as,

$$\sigma_s = \frac{L_{p,s}}{L_p} \quad \text{(Eq. 2)}$$

where $L_{p,s}$ is the apparent water permeability obtained with s as the osmolyte, in the present study NH[inf]4Cl, and L_p as the true osmotic water permeability obtained with an impermeable osmolyte, in the present study NaCl.

Electrophysiology—Conventional two-electrode voltage clamp studies were performed with a DAGAN CA-1B High Performance oocyte clamp (DAGAN, Minneapolis, MN) with DigiData 1322A interface controlled by pCLAMP software, version 9.2 (Axon Instruments, Burlingame, CA). The membrane potential was clamped at −50 mV and the current-voltage (I/V) relationship was determined by stepping the clamp potential from −50 mV to test potentials ranging from +40 mV to −120 mV in 20-mV increments (100-ms pulses). Currents measured at the holding potential were sampled at 5 Hz, and currents measured at the test potentials were low pass-filtered at 1 kHz and sampled at 2 kHz.

Intracellular pH Measurements—Changes in pH_i in oocytes were determined with ion-selective microelectrodes under voltage-clamp conditions. For measurement of intracellular pH and membrane potential, double-barreled microelectrodes were used; the manufacture and application have been described in detail previously (62). Electrodes were superfused with control solution (100 mM NaCl, 2 mM KCl, 1 mM $CaCl_2$, 1 mM $MgCl_2$, 10 mM HEPES, pH 7.4) for calibration, and after a stable electrode potential was reached, control solution pH 7.0 was applied until the electrode again reached a stable potential. The subsequent measurements of oocyte pH_i were stored digitally using homemade phosphocholine software. For two-electrode voltage clamp, a borosilicate glass capillary, 1.5 mm in diameter, was pulled to a micropipette and backfilled with 3 M KCl. This electrode was used for current injection and was connected to the head-stage of an Axoclamp 2A amplifier (Molecular Devices, Sunnyvale, CA). The actual membrane voltage was recorded by the reference barrel of the double-barreled pH-sensitive microelectrode. Oocytes were clamped to a holding potential of −40 mV. A stable pH_i baseline was obtained in control solution (100 mM NaCl, 2 mM KCl, 1 mM $CaCl_2$, 1 mM $MgCl_2$, 10 mM choline chloride, 10 mM HEPES, pH 7.4) before exposure of the oocytes to an isosmotic solution containing 10 mM NH_4Cl replacing choline chloride. Optimal pH_i changes were detected when the ion-selective electrode was located near the inner surface of the plasma membrane as described previously (63).

Molecular Dynamics Simulations—Molecular dynamics simulations were carried out with the software GROMACS 5.0

(64). The CHARMM36 force field was used for the AQP4 protein, ions, ammonia, ammonium, and the lipid parameters (65). The AQP4 protein was embedded in a patch with 361 POPC lipids and was solvated with ~27,000 CHARMM TIP3P explicit water molecules (66). The choice of the lipids was motivated by phosphocholine lipids (with mixed saturated-unsaturated tails) as the dominant lipids in eukaryotic cell membranes (67). Throughout the simulations, temperature and pressure were maintained at 310 K, 5 degrees above the lipid critical temperature and at 1 atm with a v-rescale thermostat and a Parrinello-Rahman barostat (68). An ionic strength of 150 mM NaCl was maintained to mimic physiological conditions. Explicit electrostatics were used with the Particle Mesh Ewald method for simulating long range interactions (69) with a cut-off of 1.2 nm, whereas the short range van der Waals interactions were simulated using a shift function with a switch at 0.8 nm and the cutoff at 1 nm. The crystal structure with a resolution of 0.18 nm (PDB code 3GD8) was used as the protein model (70). The package WHATIF (71) was used to predict the protonation of the protein residues at neutral pH conditions. Later analysis was carried out using GROMACS tools, the MDANALYSIS library (72), and the HOLE2.0 suite of programs (73).

Umbrella Sampling Simulations—To calculate the free energy profile of ammonia across the AQP4 channel, we used the US-enhanced sampling technique, as implemented in GROMACS. We used the WHAM algorithm to calculate the resulting PMF, and the statistical uncertainty associated with it was calculated via bootstrapping (74). To have unambiguous comparison between multiple profiles, we used a radial flat bottom potential as implemented in GROMACS 5.0 to constrain the ammonia molecule subjected to umbrella "pulling." This allowed us to take into account entropic and concentration effects of entering the channel from a given "bulk" volume surrounding the channel. The sampling itself was carried out with 280 windows, spread across 7 nm across and beyond the channel, with each window as small as 0.025 nm. A harmonic force of 500 $kJ{\cdot}mol^{-1}{\cdot}nm^{-1}$ was used to restrain the ammonia molecule in a given window. Each window was simulated for 6 ns, of which the first nanosecond was discarded during analysis to account for equilibration.

Statistics—Data are presented as the means ± S.E. Student's *t* test or analysis of variance with Šidák's multiple comparison post hoc test were used for the statistical analysis (GraphPrism 6.0, GraphPad, CA). A probability level of $p < 0.05$ was considered statistically significant. All oocyte experiments were carried out on individual oocytes obtained from at least three different animal donors.

Author Contributions—N. M. and M. A. designed, performed, and analyzed the experiments shown in Figs 2 and 4. B. L. de G. and S. K. designed, performed, and analyzed the experiments shown in Figs. 5–7. J. W. D. and H. P. S. designed, performed, and analyzed the experiments shown in Fig. 3. N. M., M. A., B. L. de G., and S. K. wrote the majority of the paper.

Acknowledgments—We greatly value the technical assistance provided by Charlotte Goos Iversen and Catia Correa Goncalves Andersen.

References

1. Rangroo Thrane, V., Thrane, A. S., Wang, F., Cotrina, M. L., Smith, N. A., Chen, M., Xu, Q., Kang, N., Fujita, T., Nagelhus, E. A., and Nedergaard, M. (2013) Ammonia triggers neuronal disinhibition and seizures by impairing astrocyte potassium buffering. *Nat. Med.* **19,** 1643–1648
2. Butterworth, R. F. (2002) Pathophysiology of hepatic encephalopathy: a new look at ammonia. *Metab. Brain Dis.* **17,** 221–227
3. Butterworth, R. F., Giguere, J. F., Michaud, J., Lavoie, J., and Layrargues, G. P. (1987) Ammonia: key factor in the pathogenesis of hepatic encephalopathy. *Neurochem. Pathol.* **6,** 1–12
4. Laursen, H., and Diemer, N. H. (1980) Morphometry of astrocyte and oligodendrocyte ultrastructure after portocaval anastomosis in the rat. *Acta Neuropathol.* **51,** 65–70
5. Cohn, R. M., and Roth, K. S. (2004) Hyperammonemia, bane of the brain. *Clin. Pediatr. (Phila.)* **43,** 683–689
6. Caner, T., Abdulnour-Nakhoul, S., Brown, K., Islam, M. T., Hamm, L. L., and Nakhoul, N. L. (2015) Mechanisms of ammonia and ammonium transport by rhesus-associated glycoproteins. *Am. J. Physiol. Cell Physiol.* **309,** C747–C758
7. Choe, H., Sackin, H., and Palmer, L. G. (2000) Permeation properties of inward-rectifier potassium channels and their molecular determinants. *J. Gen. Physiol.* **115,** 391–404
8. Chepilko, S., Zhou, H., Sackin, H., and Palmer, L. G. (1995) Permeation and gating properties of a cloned renal K^+ channel. *Am. J. Physiol.* **268,** C389–C401
9. Zhou, H., Tate, S. S., and Palmer, L. G. (1994) Primary structure and functional properties of an epithelial K channel. *Am. J. Physiol.* **266,** C809–C824
10. Edvinsson, J. M., Shah, A. J., and Palmer, L. G. (2011) Kir4.1 K^+ channels are regulated by external cations. *Channels* **5,** 269–279
11. Bachmann, O., Wüchner, K., Rossmann, H., Leipziger, J., Osikowska, B., Colledge, W. H., Ratcliff, R., Evans, M. J., Gregor, M., and Seidler, U. (2003) Expression and regulation of the Na^+-K^+-$2Cl^-$ cotransporter NKCC1 in the normal and CFTR-deficient murine colon. *J. Physiol.* **549,** 525–536
12. Bergeron, M. J., Gagnon, E., Wallendorff, B., Lapointe, J. Y., and Isenring, P. (2003) Ammonium transport and pH regulation by K^+-Cl^- cotransporters. *Am. J. Physiol. Renal Physiol.* **285,** F68–F78
13. Kinne, R., Kinne-Saffran, E., Schütz, H., and Schölermann, B. (1986) Ammonium transport in medullary thick ascending limb of rabbit kidney: involvement of the Na^+,K^+,Cl^- cotransporter. *J. Membr. Biol.* **94,** 279–284
14. Kurtz, I., and Balaban, R. S. (1986) Ammonium as a substrate for Na^+-K^+-ATPase in rabbit proximal tubules. *Am. J. Physiol.* **250,** F497–F502
15. Watts, B. A., 3rd, and Good, D. W. (1994) Effects of ammonium on intracellular pH in rat medullary thick ascending limb: mechanisms of apical membrane NH_4^+ transport. *J. Gen. Physiol.* **103,** 917–936
16. Blatz, A. L., and Magleby, K. L. (1984) Ion conductance and selectivity of single calcium-activated potassium channels in cultured rat muscle. *J. Gen. Physiol.* **84,** 1–23
17. Hamm, L. L., Trigg, D., Martin, D., Gillespie, C., and Buerkert, J. (1985) Transport of ammonia in the rabbit cortical collecting tubule. *J. Clin. Invest.* **75,** 478–485
18. Boron, W. F., Waisbren, S. J., Modlin, I. M., and Geibel, J. P. (1994) Unique permeability barrier of the apical surface of parietal and chief cells in isolated perfused gastric glands. *J. Exp. Biol.* **196,** 347–360
19. Yip, K. P., and Kurtz, I. (1995) NH_3 permeability of principal cells and intercalated cells measured by confocal fluorescence imaging. *Am. J. Physiol.* **269,** F545–F550
20. Loqué, D., Ludewig, U., Yuan, L., and von Wirén, N. (2005) Tonoplast intrinsic proteins AtTIP2;1 and AtTIP2;3 facilitate NH_3 transport into the vacuole. *Plant Physiol.* **137,** 671–680
21. Jahn, T. P., Møller, A. L., Zeuthen, T., Holm, L. M., Klaerke, D. A., Mohsin, B., Kühlbrandt, W., and Schjoerring, J. K. (2004) Aquaporin homologues in plants and mammals transport ammonia. *FEBS Lett.* **574,** 31–36
22. Holm, L. M., Jahn, T. P., Møller, A. L., Schjoerring, J. K., Ferri, D., Klaerke, D. A., and Zeuthen, T. (2005) NH_3 and NH_4^+ permeability in aquaporin-expressing *Xenopus* oocytes. *Pflugers Arch.* **450,** 415–428

23. Dynowski, M., Mayer, M., Moran, O., and Ludewig, U. (2008) Molecular determinants of ammonia and urea conductance in plant aquaporin homologs. *FEBS Lett.* **582,** 2458–2462
24. Bertl, A., and Kaldenhoff, R. (2007) Function of a separate NH_3-pore in Aquaporin TIP2;2 from wheat. *FEBS Lett.* **581,** 5413–5417
25. Hwang, J. H., Ellingson, S. R., and Roberts, D. M. (2010) Ammonia permeability of the soybean nodulin 26 channel. *FEBS Lett.* **584,** 4339–4343
26. Zeuthen, T., Wu, B., Pavlovic-Djuranovic, S., Holm, L. M., Uzcategui, N. L., Duszenko, M., Kun, J. F., Schultz, J. E., and Beitz, E. (2006) Ammonia permeability of the aquaglyceroporins from *Plasmodium falciparum*, *Toxoplasma gondii*, and *Trypanosoma brucei*. *Mol. Microbiol.* **61,** 1598–1608
27. Benga, O., and Huber, V. J. (2012) Brain water channel proteins in health and disease. *Mol. Aspects Med.* **33,** 562–578
28. Gomes, D., Agasse, A., Thiébaud, P., Delrot, S., Gerós, H., and Chaumont, F. (2009) Aquaporins are multifunctional water and solute transporters highly divergent in living organisms. *Biochim. Biophys. Acta* **1788,** 1213–1228
29. Musa-Aziz, R., Chen, L. M., Pelletier, M. F., and Boron, W. F. (2009) Relative CO_2/NH_3 selectivities of AQP1, AQP4, AQP5, AmtB, and RhAG. *Proc. Natl. Acad. Sci. U.S.A.* **106,** 5406–5411
30. Nakhoul, N. L., Hering-Smith, K. S., Abdulnour-Nakhoul, S. M., and Hamm, L. L. (2001) Transport of NH_3/NH in oocytes expressing aquaporin-1. *Am. J. Physiol. Renal Physiol.* **281,** F255–F263
31. Geyer, R. R., Musa-Aziz, R., Qin, X., and Boron, W. F. (2013) Relative CO_2/NH_3 selectivities of mammalian aquaporins 0–9. *Am. J. Physiol. Cell Physiol.* **304,** C985–C994
32. Beitz, E., Wu, B., Holm, L. M., Schultz, J. E., and Zeuthen, T. (2006) Point mutations in the aromatic/arginine region in aquaporin 1 allow passage of urea, glycerol, ammonia, and protons. *Proc. Natl. Acad. Sci. U.S.A.* **103,** 269–274
33. Vilas, G. L., Loganathan, S. K., Liu, J., Riau, A. K., Young, J. D., Mehta, J. S., Vithana, E. N., and Casey, J. R. (2013) Transmembrane water-flux through SLC4A11: a route defective in genetic corneal diseases. *Hum. Mol. Genet.* **22,** 4579–4590
34. Zhang, W., Ogando, D. G., Bonanno, J. A., and Obukhov, A. G. (2015) Human SLC4A11 is a novel NH_3/H^+ co-transporter. *J. Biol. Chem.* **290,** 16894–16905
35. Swain, M., Butterworth, R. F., and Blei, A. T. (1992) Ammonia and related amino acids in the pathogenesis of brain edema in acute ischemic liver failure in rats. *Hepatology* **15,** 449–453
36. Lockwood, A. H., Murphy, B. W., Donnelly, K. Z., Mahl, T. C., and Perini, S. (1993) Positron-emission tomographic localization of abnormalities of brain metabolism in patients with minimal hepatic encephalopathy. *Hepatology* **18,** 1061–1068
37. Rose, C. (2006) Effect of ammonia on astrocytic glutamate uptake/release mechanisms. *J. Neurochem.* **97,** 11–15
38. Rose, C., Kresse, W., and Kettenmann, H. (2005) Acute insult of ammonia leads to calcium-dependent glutamate release from cultured astrocytes, an effect of pH. *J. Biol. Chem.* **280,** 20937–20944
39. Søgaard, R., Novak, I., and MacAulay, N. (2012) Elevated ammonium levels: differential acute effects on three glutamate transporter isoforms. *Am. J. Physiol. Cell Physiol.* **302,** C880–C891
40. Norenberg, M. D., Rao, K. V., and Jayakumar, A. R. (2005) Mechanisms of ammonia-induced astrocyte swelling. *Metab. Brain Dis.* **20,** 303–318
41. O'Carroll, R. E., Hayes, P. C., Ebmeier, K. P., Dougall, N., Murray, C., Best, J. J., Bouchier, I. A., and Goodwin, G. M. (1991) Regional cerebral blood flow and cognitive function in patients with chronic liver disease. *Lancet* **337,** 1250–1253
42. Nielsen, S., Nagelhus, E. A., Amiry-Moghaddam, M., Bourque, C., Agre, P., and Ottersen, O. P. (1997) Specialized membrane domains for water transport in glial cells: high-resolution immunogold cytochemistry of aquaporin-4 in rat brain. *J. Neurosci.* **17,** 171–180
43. Bodega, G., Suárez, I., López-Fernández, L. A., García, M. I., Köber, M., Penedo, M., Luna, M., Juárez, S., Ciordia, S., Oria, M., Córdoba, J., and Fernández, B. (2012) Ammonia induces aquaporin-4 rearrangement in the plasma membrane of cultured astrocytes. *Neurochem. Int.* **61,** 1314–1324
44. Rama Rao, K. V., Chen, M., Simard, J. M., and Norenberg, M. D. (2003) Increased aquaporin-4 expression in ammonia-treated cultured astrocytes. *Neuroreport* **14,** 2379–2382
45. Liu, K., Nagase, H., Huang, C. G., Calamita, G., and Agre, P. (2006) Purification and functional characterization of aquaporin-8. *Biol. Cell* **98,** 153–161
46. Saparov, S. M., Liu, K., Agre, P., and Pohl, P. (2007) Fast and selective ammonia transport by aquaporin-8. *J. Biol. Chem.* **282,** 5296–5301
47. Meinild, A. K., Klaerke, D. A., and Zeuthen, T. (1998) Bidirectional water fluxes and specificity for small hydrophilic molecules in aquaporins 0–5. *J. Biol. Chem.* **273,** 32446–32451
48. Fenton, R. A., Moeller, H. B., Zelenina, M., Snaebjornsson, M. T., Holen, T., and MacAulay, N. (2010) Differential water permeability and regulation of three aquaporin 4 isoforms. *Cell. Mol. Life Sci.* **67,** 829–840
49. Hub, J. S., Winkler, F. K., Merrick, M., and de Groot, B. L. (2010) Potentials of mean force and permeabilities for carbon dioxide, ammonia, and water flux across a rhesus protein channel and lipid membranes. *J. Am. Chem. Soc.* **132,** 13251–13263
50. Kirscht, A., Kaptan, S. S., Bienert, G. P., Chaumont, F., Nissen, P., de Groot, B. L., Kjellbom, P., Gourdon, P., and Johanson, U. (2016) crystal structure of an ammonia-permeable aquaporin. *PLoS Biol.* **14,** e1002411
51. Burckhardt, B. C., and Frömter, E. (1992) Pathways of NH_3/ NH_4^+ permeation across *Xenopus laevis* oocyte cell membrane. *Pflugers Archiv.* **420,** 83–86
52. Boldt, M., Burckhardt, G., and Burckhardt, B. C. (2003) NH_4^+ conductance in *Xenopus laevis* oocytes. III. Effect of NH_3. *Pflugers Archiv.* **446,** 652–657
53. Cougnon, M., Bouyer, P., Hulin, P., Anagnostopoulos, T., and Planelles, G. (1996) Further investigation of ionic diffusive properties and of NH_4^+ pathways in *Xenopus laevis* oocyte cell membrane. *Pflugers Archiv.* **431,** 658–667
54. Sasaki, S., Ishibashi, K., Nagai, T., and Marumo, F. (1992) Regulation mechanisms of intracellular pH of *Xenopus laevis* oocyte. *Biochim. Biophys. Acta* **1137,** 45–51
55. Burckhardt, B. C., and Burckhardt, G. (1997) NH_4^+ conductance in *Xenopus laevis* oocytes. I. Basic observations. *Pflugers Archiv.* **434,** 306–312
56. Hub, J. S., and de Groot, B. L. (2008) Mechanism of selectivity in aquaporins and aquaglyceroporins. *Proc. Natl. Acad. Sci. U.S.A.* **105,** 1198–1203
57. Bak, L. K., Schousboe, A., and Waagepetersen, H. S. (2006) The glutamate/GABA-glutamine cycle: aspects of transport, neurotransmitter homeostasis, and ammonia transfer. *J. Neurochem.* **98,** 641–653
58. Wolburg, H. (1995) Orthogonal arrays of intramembranous particles: a review with special reference to astrocytes. *J. Hirnforsch.* **36,** 239–258
59. Adeva, M. M., Souto, G., Blanco, N., and Donapetry, C. (2012) Ammonium metabolism in humans. *Metab. Clin. Exp.* **61,** 1495–1511
60. Zeuthen, T., Belhage, B., and Zeuthen, E. (2006) Water transport by Na^+-coupled cotransporters of glucose (SGLT1) and of iodide (NIS): the dependence of substrate size studied at high resolution. *J. Physiol.* **570,** 485–499
61. Zampighi, G. A., Kreman, M., Boorer, K. J., Loo, D. D., Bezanilla, F., Chandy, G., Hall, J. E., and Wright, E. M. (1995) A method for determining the unitary functional capacity of cloned channels and transporters expressed in *Xenopus laevis* oocytes. *J. Membr. Biol.* **148,** 65–78
62. Deitmer, J. W. (1991) Electrogenic sodium-dependent bicarbonate secretion by glial cells of the leech central nervous system. *J. Gen. Physiol.* **98,** 637–655
63. Bröer, S., Schneider, H. P., Bröer, A., Rahman, B., Hamprecht, B., and Deitmer, J. W. (1998) Characterization of the monocarboxylate transporter 1 expressed in *Xenopus laevis* oocytes by changes in cytosolic pH. *Biochem. J.* **333,** 167–174
64. Abraham, M. J., Murtola, T., Schulz, R., Pall, S., Smith, J. C., Hess, B., and Lindahl, E. (2015) GROMACS: high performance molecular simulations through multi-level parallelism from laptops to supercomputers. *SoftwareX* **1–2,** 19–25
65. Huang, J., and MacKerell, A. D., Jr.(2013) CHARMM36 all-atom additive protein force field: validation based on comparison to NMR data. *J. Comput. Chem.* **34,** 2135–2145
66. Jorgensen, W. L., Chandrasekhar, J., Madura, J. D., Impey, R. W., and Klein, M. L. (1983) Comparison of simple potential functions for simulating liquid water. *J. Chem. Phys.* **79,** 926–935

67. van Meer, G., Voelker, D. R., and Feigenson, G. W. (2008) Membrane lipids: where they are and how they behave. *Nat. Rev. Mol. Cell Biol.* **9,** 112–124
68. Bussi, G., Donadio, D., and Parrinello, M. (2007) Canonical sampling through velocity rescaling. *J. Chem. Phys.* **126,** 014101
69. Darden, T., York, D., and Pedersen, L. (1993) Particle mesh Ewald: an N. log(N) method for Ewald sums in large systems. *J. Chem. Phys.* **98,** 10089–10092
70. Ho, J. D., Yeh, R., Sandstrom, A., Chorny, I., Harries, W. E., Robbins, R. A., Miercke, L. J., and Stroud, R. M. (2009) Crystal structure of human aquaporin 4 at 1.8 angstrom and its mechanism of conductance. *Proc. Natl. Acad. Sci. U.S.A.* **106,** 7437–7442
71. Vriend, G. (1990) What if: a molecular modeling and drug design program. *J. Mol. Graph.* **8,** 52–56
72. Michaud-Agrawal, N., Denning, E. J., Woolf, T. B., and Beckstein, O. (2011) Software news and updates MDAnalysis: a toolkit for the analysis of molecular dynamics simulations. *J. Comput. Chem.* **32,** 2319–2327
73. Smart, O. S., Goodfellow, J. M., and Wallace, B. A. (1993) The pore dimensions of gramicidin-A. *Biophys. J.* **65,** 2455–2460
74. Hub, J. S., Aponte-Santamaría, C., Grubmüller, H., and de Groot, B. L. (2010) Voltage-regulated water flux through aquaporin channels *in silico*. *Biophys. J.* **99,** L97–L99